DOI: 10.1002/chem.200700235

Beyond the Structure–Property Relationship Paradigm: Influence of the Crystal Structure and Microstructure on the Li^+ Conductivity of $La_{2/3}Li_xTi_{1-x}Al_xO_3$ Oxides

Susana García-Martín,[b] Ainhoa Morata-Orrantía,[b] Miguel A. Alario-Franco,[b] Juan Rodríguez-Carvajal,[c, d] and Ulises Amador*[a]

Abstract: The crystal structures of several oxides of the $La_{2/3}Li_xTi_{1-x}Al_xO_3$ system have been studied by selected-area electron diffraction, high-resolution transmission electron microscopy, and powder neutron diffraction, and their lithium conductivity has been by complex impedance spectroscopy. The compounds have a perovskite-related structure with a unit cell $\sqrt{2}a_p \times 2a_p \times \sqrt{2}a_p$ (a_p = perovskite lattice parameter) due to the tilting of the $(Ti/Al)O_6$ octahedra and the ordering of lanthanum and lithium ions and vacancies along the $2a_p$ axis. The Li^+ ions present a distorted square-planar coordination and are located in interstitial positions of the structure, which could explain the very high ionic conductivity of this type of material. The lithium conductivity depends on the oxide composition and its crystal microstructure, which varies with the thermal treatment of the sample. The microstructure of these titanates is complex due to formation of domains of ordering and other defects such as strains and compositional fluctuations.

Keywords: microstructure · neutron diffraction · perovskite phases · solid-state structures · structure–property relationships · titanates

Introduction

Structure–property relationships are a well-established paradigm in solid-state chemistry and materials science.[1] Among the uncountable examples of the sort, ionic conductivity is considered as a prime one.

It is evident that some structures facilitate, while some others complicate, ionic diffusion and conductivity. The much studied perovskite structure (ABO_3) has very often been the material substrate for making good ionic conductors and, in particular, lithium has been shown to move in some perovskite systems faster than in any other materials.

The very high value of lithium conductivity ($\sigma_{bulk} \sim 1 \times 10^3\ S\,cm^{-1}$ at room temperature) reported in the literature some years ago for the oxides of general formula $La_{2/3-x}Li_{3x}TiO_3$[2–6] has indeed developed a great interest in the study of this kind of titanate with perovskite-related structures. In this sense, substitution of La and/or Ti by other metal ions has lead to the discovery of a multitude of new systems with different properties according to the type and degree of substitution.[7]

Among the systems obtained by substitution of Ti in the lithium–lanthanide–titanates is the $La_{2/3}Li_xTi_{1-x}Al_xO_3$ ($0.06 \leq x \leq 0.3$) system,[8] which also has a very high lithium conductivity, though significantly lower than the $La_{2/3-x}Li_{3x}TiO_3$ oxides. We believe that the reason for having lower conductivity is that the optimum charge carriers/A-cation vacancies ratio is not achieved in the $La_{2/3}Li_xTi_{1-x}Al_xO_3$ system, but rather that of $La_{0.56}Li_{0.33+x}Ti_{1-x}Al_xO_3$, which has the highest lithium conductivity reported to date in the literature for a

[a] Prof. U. Amador
Departamento de Química, Facultad de Farmacia
Universidad CEU-San Pablo, 28668-Boadilla del Monte
Madrid (Spain)
Fax: (+34) 91-351-0475
E-mail: uamador@ceu.es

[b] Dr. S. García-Martín, A. Morata-Orrantía, Dr. M. A. Alario-Franco
Departamento de Química Inorgánica
Facultad de Ciencias Químicas Universidad Complutense
28040-Madrid (Spain)

[c] Dr. J. Rodríguez-Carvajal
Laboratoire Léon Brillouin (CEA-CNRS)
Centre d'Etudes de Saclay, 91191 Gif-sur-Yvette Cedex (France)

[d] Dr. J. Rodríguez-Carvajal
Present address: Institut Laue-Langevin
BP 156–38042 Grenoble Cedex 9 (France)

Supporting information for this article is available on the WWW under http://www.chemeurj.org/ or from the author.

crystalline material ($\sigma_{bulk} \sim 2.95 \times 10^3$ S cm^{-1} at 295 K for $x = 0.03$).[9] Another interesting property of the $La_{2/3}Li_xTi_{1-x}Al_xO_3$ oxides is their dielectric behavior. We have recently reported "giant" barrier layer capacitance effects in $La_{0.67}Li_{0.25}Ti_{0.75}Al_{0.25}O_3$.[10]

The chemical and physical properties of materials are intimately related to their crystal structure and microstructure. Therefore, the knowledge of the crystal structure of these oxides, in particular the location of the Li ions, is essential to understand their physicochemical behavior. Moreover, microstructural effects, such as domain formation, may affect the Li^+-motion pathways and hence the ionic conductivity of these oxides. Besides, it is known that the profile of the powder diffraction patterns (either X-ray or neutron) is substantially affected by the microstructure of the crystalline solids; consequently the knowledge of the crystal microstructure is essential for solving the real as opposed to the average structure of the solids.

We have recently reported a study of the crystal structure and microstructure of two $La_{2/3-x}Li_{3x}TiO_3$ oxides by the complementary use of electron diffraction and transmission electron microscopy and powder synchrotron X-ray diffraction.[11] In that work, we solved the structure of our materials taking into account, simultaneously, the effects of their microstructure and defects on the diffraction patterns.

In present work, we use this approach for obtaining detailed structural features of our oxides. Since some physical properties of these titanates vary with their microstructure, it is important to establish the relationships between composition, crystal structure, microstructure, and properties, in particular their ionic conductivity.

Therefore, here we present the study of the crystal structure and microstructure of some $La_{2/3}Li_xTi_{1-x}Al_xO_3$ oxides by means of powder neutron diffraction (PND), powder X-ray diffraction (PXRD), selected-area electron diffraction (SAED) and high-resolution transmission electron microscopy (HRTEM), as well as the dependence of Li-ion conductivity on the crystal structure and microstructure.

Results and Discussion

Previous work indicates modifications of the XRD patterns of the $La_{2/3}Li_xTi_{1-x}Al_xO_3$ oxides ($0.06 \le x \le 0.3$) with both the composition and the annealing temperature.[8] Superlattice reflections with respect to the ideal cubic perovskite structure are relatively sharp in the patterns of the samples with $0.06 \le x \le 0.2$ annealed and quenched from 1273 K. These extra reflections broaden when x increases in such a way that they are almost invisible in the sample corresponding to $x = 0.3$. The superlattice reflections also broaden when increasing the annealing temperature; in fact, they almost disappear for the sample with $x = 0.2$ when it is annealed at 1573 K and quenched from this temperature.

Despite the differences observed by PXRD, all the oxides have the same basic unit cell ($a \sim \sqrt{2}a_p$, $b \sim \sqrt{2}a_p$, $c \sim 2a_p$; a_p = perovskite lattice parameter) and their crystals are formed by three sets of domains with different orientations of this unit cell.[8] However, the size of the domains depends on the composition and the thermal history of the sample. It appears that the intensity of the superlattice reflections in the PXRD patterns is related to the size of the domains in such a way that, broad (almost invisible) peaks are due to a microdomain microstructure and sharp peaks correspond to relatively large domains.

In the following we present the structural and microstructural characterization at room temperature of $La_{2/3}Li_xTi_{1-x}Al_xO_3$ samples corresponding to $x = 0.1$ and 0.2, both of them annealed and quenched from 1273 K (samples 01 LT and 02 LT, respectively) and from 1573 K (samples 01 HT and 02 HT), and the oxide with $x = 0.3$ annealed and quenched from 1273 K (sample 03 LT). The sample 01 HT was also studied at low temperature (2 K) to determine the static or dynamic nature of the structural disorder observed in these compounds. In addition, the electrical characterization of these materials is also presented.

Transmission electron microscopy (TEM) and high-resolution TEM (HRTEM): Figure 1 shows three different SAED patterns of sample 03 LT. Extra reflections with respect to

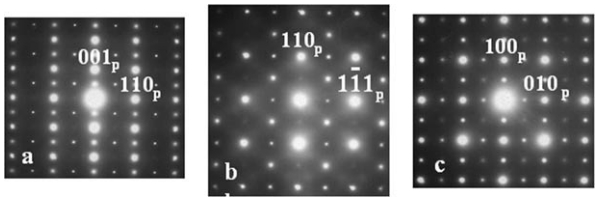

Figure 1. SAED patterns of sample 03 LT along the a) $[\bar{1}10]_p$, b) $[1\bar{1}\bar{2}]_p$, and c) $[001]_p$ zone axes.

the ideal cubic perovskite structure are almost invisible in the PXRD patterns of this sample. However, the $(00l/2)_p$, $(h/2h/2l/2)_p$, $(h/2h/2l)_p$, $(h/200)_p$, and $(0k/20)_p$ superlattice reflections are observed in the SAED patterns (the main Bragg reflections have been indexed according to the ideal perovskite structure), which correspond to a crystal unit cell of dimensions $2a_p \times 2a_p \times 2a_p$ or alternatively to the formation of domains of $\sqrt{2}a_p \times \sqrt{2}a_p \times 2a_p$ unit cell with the long $2a_p$ axis oriented along three mutually perpendicular directions. TEM has to be used to distinguish between these two possibilities.

Figure 2a shows the HRTEM image corresponding to the $[001]_p$ zone axis. Contrast differences with periodicity $\sim 2a_p$ are observed in small regions of the crystal (with two or three times the size of the unit cell dimensions) along either the $[100]_p$ or the $[010]_p$ directions, but never in the two directions simultaneously (this would correspond to a $2a_p \times 2a_p \times 2a_p$ unit cell). Therefore, the crystal is formed by microdomains of the $\sqrt{2}a_p \times \sqrt{2}a_p \times 2a_p$ cell with different orientations of the long $2a_p$ axis.

The SAED patterns for all the oxides of the $La_{2/3}Li_xTi_{1-x}Al_xO_3$ system are similar to those shown in Figure 1, with no

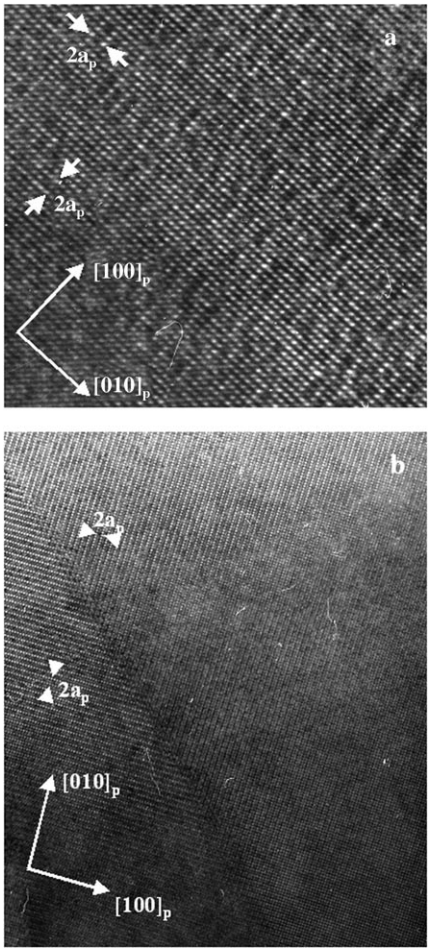

Figure 2. HRTEM image corresponding to the $[001]_p$ zone axis of a) sample 03 LT and b) sample 01 LT.

dependence on either the composition or the annealing temperature of the samples. However, the size of the ordering domains varies with these two factors, in such a way that the crystals of samples 01 LT and 01 HT ($x=0.1$) have big domains (Figure 2b); the crystals of the oxide with $x=0.2$ are formed by large domains when annealed and quenched from 1273 K (sample 02 LT) and microdomains for sample 02 HT (quenched from 1573 K), whereas the crystals with $x=0.3$ always have microdomain formation.

It must also be mentioned that splitting of the (hhl) reflections is observed in the SAED patterns at high diffraction angles (not seen in Figure 1 due to insufficient magnification). This is due to slightly different dimensions of the a and b lattice parameters and domain formation, indicating that the symmetry of the crystal structure of these compounds must be orthorhombic or monoclinic.

Therefore, none of the crystal structure models most recently proposed by other authors for several compounds of the $La_{2/3-x}Li_{3x}TiO_3$ system[12–14] are valid for our $La_{2/3}Li_xTi_{1-x}Al_xO_3$ oxides because they are not based on the observed $\sim\sqrt{2}a_p\times\sqrt{2}a_p\times 2a_p$ cell, but on a $\sim 2a_p\times 2a_p\times 2a_p$ one. In fact, none of these models agrees with the crystal microstructure of the $La_{2/3-x}Li_{3x}TiO_3$ oxides observed by SAED and TEM.[11,15,16]

Finally the extensive study carried out by TEM allows us to conclude that neither secondary phases nor amorphous materials are present in the samples in significant quantities.

Crystal structure refinement

Room temperature structure: Although there are many investigations devoted to materials of the $La_{2/3-x}Li_{3x}TiO_3$ family, the model for describing the structure of these compounds is still an open and controversial question.

To properly determine the structure of complex materials, as is the perovskite-like $La_{2/3-x}Li_xTiO_3$ family, averaging (PXRD and PND) and local techniques (such as SAED and HRTEM) must be combined. Only by doing so can a complete and adequate structural model be developed.

$La_{2/3-x}Li_{3x}TiO_3$ materials, and related ones, present a complex microstructure that makes the analysis of their diffraction patterns (XRD and NPD) a difficult task. Thus, unrealistic or unnecessarily complex models have been proposed for describing the average (ideal) structure of these materials. In a previous paper[11] we demonstrated that different samples of the $La_{1/2+x}Li_{1/2-3x}TiO_3$ series presented the same unit cell, the so-called "diagonal cell" ($a\sim\sqrt{2}a_p$, $b\sim\sqrt{2}a_p$, $c\sim 2a_p$) and symmetry (*Pmma* or *P*..2/*m* when additional distortion occurs), in spite of having quite different PXRD patterns that may suggest different unit cells and/or symmetry.

We are now going to follow the above underlined method for refining the crystal structure of our $La_{2/3}Li_xTi_{1-x}Al_xO_3$ oxides.

There are only four octahedra-tilting systems in perovskites that originate a diagonal unit cell: these are $a^0a^0c^-$, $a^0b^-b^-$; $a^+b^-b^-$, and $a^+b^-c^-$ (Glazer's notation),[17–19] corresponding to the space groups *I*4/*mcm*, *Imma*, *Pnma*, and $P2_1/m$, respectively. In addition to the octahedral tilting, the ordering of lanthanum and lithium atoms as well as the vacancies along the $2a_p$ axis must be considered; otherwise the ($00l/2$) reflections will be too weak to be observed by PXRD, discarding the *I*-centered groups (however, the *I*4/*mcm* symmetry has recently been used to refine the structure of $Li_{0.3}La_{0.567}TiO_3$ from time-of-flight (TOF) neutron diffraction data).[20] Taking into account that tetragonal groups or subgroups of the above space groups can be discarded because our oxides are either orthorhombic or monoclinic (splitting of the (hhl) reflections), we deduce that the *P*2*ma* symmetry resulting from ordering in the $a^+b^-b^-$ tilting system and the *Pmma* and *P*..2/*m* symmetry resulting from the ordering in the $a^-b^0a^-$ one (with unit cell setting $a\sim\sqrt{2}a_p$, $b\sim 2a_p$, $c\sim\sqrt{2}a_p$) are compatible with the reflections in the SAED patterns. It should be noted that the extinctions due to the *a*-glide plane and the screw axis are not observed due to the domain microstructure of the materials.

Although the structure of the sample 01 LT could be monoclinic, like $La_{0.6}Li_{0.2}TiO_3$ annealed and quenched from 1273 K,[11] PND data have not enough resolution to detect the slight distortion responsible for the lack of the ortho-

rhombic symmetry (*Pmma*). However, we tried structural models of *Pmma*, $P2_1/m$, and *P2ma* symmetries; despite the last two models having more parameters, the refinements did not improve and became unstable. Thus, *Pmma* symmetry was preferred. In the Supporting Information the structural parameters are collected in Tables 1 and 2, whereas Tables 3 and 4 show the main structural information. The metal substructure is quite defective, whereas the anionic one is complete and no oxygen vacancies or interstitials were observed from neutron diffraction data.

Figure 3 shows the graphic results of the fitting of the PND diffraction patterns for samples 01 LT and 03 LT. In the latter a small amount (about 3%) of $LiAl_5O_8$ is present as impurity. The actual composition of sample 03 LT (Table 1 Supporting Information) suggests that a small loss of lithium oxide was also produced during the synthesis at high temperature (1573 K) and agrees with the fact that the limit for the solid solution is close to $x=0.3$.[8]

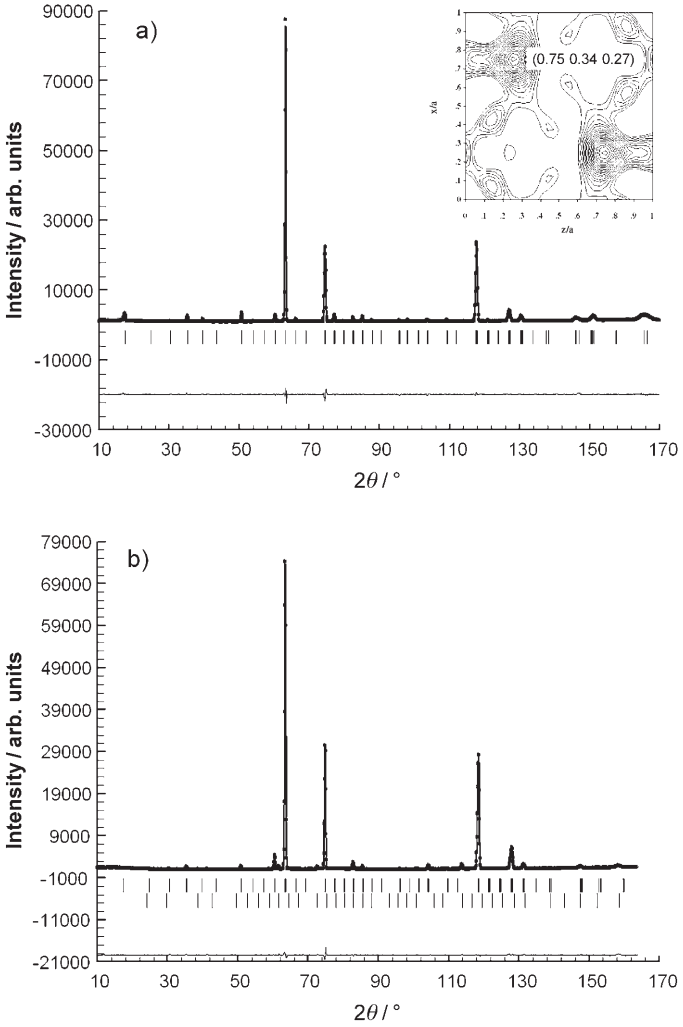

Figure 3. Experimental (points), calculated (solid line) and difference (bottom) neutron diffraction patterns recorded at room temperature for a) 01 LT and b) 03 LT. The inset in a) shows a difference Fourier density map of the plane containing lithium ions (contour levels from 0.0 to -0.019 fm Å^{-3}, 0.001 fm Å^{-3} per step; note that the Li scattering factor for a neutron is -1.9 fm). In b) the second row of vertical marks indicates the peaks of $LiAl_5O_8$ present as impurity.

Figure 4 shows a schematic representation of the crystal structure of all the $La_{2/3}Li_xTi_{1-x}Al_xO_3$ compounds investigated.

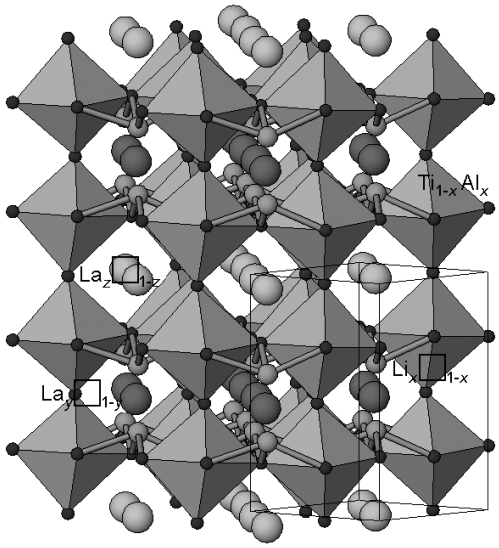

Figure 4. Schematic representation of $La_{2/3}Li_xTi_{1-x}Al_xO_3$ materials (see Tables 1 and 2 in the Supporting Information for details). Color code: large light gray spheres: La1; large dark gray spheres: La2; and small light gray spheres: lithium.

In spite of their different composition and/or thermal treatments all these materials have some common features. The formation of a superstructure of the basic perovskite is due to two mechanisms: the tilting of octahedra and the ordering of La^{3+}, Li^+, and the vacancies along the $2a_p$ axis.

The tilting system seems to be the same in all these materials, $a^0b^-b^-$, ($a^-b^0a^-$ with unit cell setting $a\sim\sqrt{2}a_p$, $b\sim 2a_p$, $c\sim\sqrt{2}a_p$ used in this work) in spite of the values of the tilting angles (Tables 3 and 4 in the Supporting Information), which seem to be significantly different. In this respect, it must be stressed that the tilting schemes usually used to describe the structures related to the ideal perovskite[17–19,21] are derived for rigid BO_6 octahedra; however, in most cases there is no reason for the octahedra to be rigid.[21] This is especially true in complex perovkites like $La_{2/3}Li_xTi_{1-x}Al_xO_3$ in which the A-sites are shared by ions of very different size and charge, such as La^{3+} and Li^+, as well as vacancies, besides, the B-sites are also shared by ions of different charge and size.[22] Hence, a more robust criterion to determine the tilting scheme is the symmetry and dimensions of the resulting unit cell. Thus, the $(Ti/Al)O_6$ octahedra are distorted (see Tables 3 and 4 in the Supporting Information) to accommodate the small lithium ions and the vacancies. It seems that the factor governing the degree of distortion of the BO_6 octahedra, and as a consequence the lowering in symmetry, is the number of vacancies in the A-sites. In this sense, the compound $La_{0.60}Li_{0.2}\square_{0.2}TiO_3$ is monoclinic ($P2/m$), whereas $La_{0.55}Li_{0.35}\square_{0.1}TiO_3$ is orthorhombic (*Pmma*).[11]

In our case, samples 01 LT and 01 HT, with composition $La_{2/3}Li_{0.1}\square_{0.23}Ti_{0.9}Al_{0.1}O_3$, could be monoclinic. Finally, the values of the tilting angles are also mainly dependent on the composition, that is, the number of vacancies in the A-site through the value of x in $La_{2/3}Li_xTi_{1-x}Al_xO_3$, in such a way that the higher the occupation of the A-sites, the larger the octahedral tilting. In contrast, the temperature of quenching has little or no effect on this structural feature. Thus, it seems that both the tilting and distortion of the BO_6 octahedra skeleton depends on the average occupation of the A-sites in the perovskite structure. As it will be discussed below, the thermal history (mainly the quenching temperature) modifies the distribution of lanthanum and lithium ions and the vacancies among the different positions they can occupy; this induces local or short-range distortions, but the average arrangement of the BO_6 octahedra is not affected.

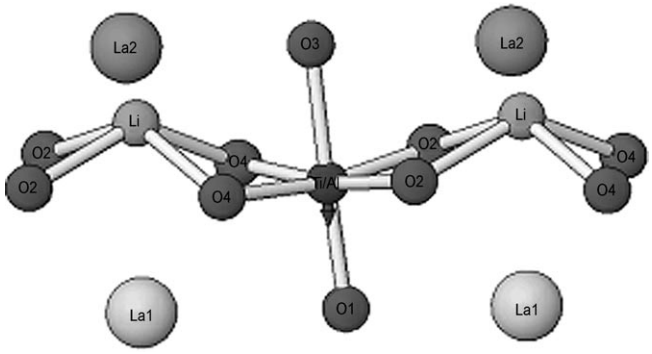

Figure 5. Detailed schematic representation of the coordination polyhedra of Li and B (Ti/Al) ions in $La_{2/3}Li_xTi_{1-x}Al_xO_3$ compounds.

In lithium ion conductors the location of these ions is of major importance. Therefore, we first obtained a refined structural model by fitting simultaneously the PND and PXRD data; then lithium ions were located by Fourier difference by using the neutron diffraction data. The inset in Figure 3a shows the density map of the plane containing lithium ions for sample 01 LT. Even for this sample with a low lithium content, the sites occupied by lithium are evident (0.75 ~ 0.34 ~ 0.27); for the other samples measured at room temperature, the lithium position is analogous. We have also considered other possible lithium locations proposed in the literature, that is, in the middle of square windows of oxygen atoms (namely (0.500.5), (0.50.50.5), (000) and (00.50)); in all cases no significant scattering density was detected for these positions in the Fourier maps and the data fitting process did not converge or became unstable. The lithium ions do not really occupy the A-sites of the perovskite structure, but interstitial positions much closer to four oxygen atoms. This could explain the very high ionic conductivity of these materials. The final refined lithium positions and occupations (once the other possible locations were discarded, the occupation of the lithium sites was refined constrained to the aluminum content) are given in Tables 1 and 2 in the Supporting Information.

Figure 5 shows the coordination polyhedron of lithium. Considering Li–O distances up to 2.5 Å, lithium is located in a square pyramid with lithium atom at the apex.

The coordination polyhedra of the lithium ions is then quite different from that proposed in the literature.[14,15,23–25] The high symmetry of the lithium coordination polyhedra in the structural model proposed by these authors seems to be due to the space group (*Cmmm*) assumed for constructing their structural model. In our model, the lithium ions are close but are not in these windows.

It is worth noting that for samples with high lithium content some significant negative density that could be assigned to lithium is also observed around the lanthanum sites. However, when fitting the PND data, the only position of lithium allowing the process to converge to a stable model was that given above. Anyhow, it cannot be totally discarded that lithium may be partially spread in the structure, mainly in the samples with higher lithium content and annealed at higher temperatures. It is a common practice to use these kinds of results to propose paths for lithium diffusion into the structure;[14] however, this must be managed with care, because the low peak-to-parameter ratio inherent to powder diffraction, the complex microstructure of these perovskites, the systematic errors, the truncation errors, and so forth make the interpretation of diffuse density in a Fourier map a controversial point. It must be remarked that nowadays scattering techniques and methods, such as Reverse Monte Carlo, exist that adequate to properly study solids with a more or less rigid arrangement and a "liquid" disordered sub-lattice.[26] This kind of study of lithium-conducting materials of the $La_{1/2+x}Li_{1/2-3x}TiO_3$ family would be of major interest.

The degree of ordering of the La^{3+} ions and vacancies along the $2a_p$ axis depends on both the annealing temperature and the composition (mainly the concentration of vacancies). However, the influence of both factors on the average composition of the two La–vacancy layers formed is quite different. While the distribution of lanthanum ions over the two positions La1 and La2 in the structure is strongly dependent on the latter factor, that is, the value of "x" (see Table 1in the Supporting Information), the annealing temperature is less important (see Tables 1 and 2 in the Supporting Information). Thus, in the sample 01 LT (with 23 % of vacancies in the A-site and quenched from 1273 K), the lanthanum-rich layers (La2) alternate with vacancy-rich (La-poor) layers (La1) along the $2a_p$ axis (Table 1 in the Supporting Information). In contrast, in 03 LT (with 3 % of vacancies also quenched from the same temperature), the composition of the two La-vacancy layers is similar (Table 1 in the Supporting Information); for an intermediate composition (13 % of vacancies in 02 LT) an intermediate situation was found. As stated above, the temperature of annealing also modifies the A-site ordering. However, its effect is less marked than that of the composition. Indeed, for the materials with low concentration of vacancies ($x \geq 0.2$ in $La_{2/3}Li_xTi_{1-x}Al_xO_3$) this effect is almost negligible.

As pointed out in our previous paper, the ordering within the A-site of the structure is related to the displacement of titanium ions from the center of the TiO_6 octahedra towards the vacancy-rich A-layers in the structure.[11] Indeed, in our case, Ti^{+4} and Al^{+3}, which share the B-site of the perovskite structure, are displaced towards the La1 layers that are vacancy-rich. In all samples quenched from 1273 K (01 LT, 02 LT, and 03 LT) and in 01 HT, the displacement of the B ions is as large as 0.08 Å, whereas in 02 HT the B ions are only displaced by 0.03 Å from the BO_6 octahedra centers. Thus, the composition of the La–vacancy layers and the displacement of B cations are closely related, in such a way that the deficiency in positive charge in the vacancy-rich layers (La1 layers) are compensated by the proximity of Ti^{+4} or Al^{3+} ions. In addition, as it will be shown below, both the displacement of the B ions and the occupation of the A-sites play a crucial role in the location of lithium ions in the structure.

As shown in Figure 4, the Li^+ positions are close to the La2 positions that define layers extending perpendicular to the $2a_p$ axis. This gives a somewhat two-dimensional character to the structure and to the lithium ionic diffusion. At a first sight it could seem quite unexpected that lithium ions occupy sites close the La2 positions, since these are more populated than the La1 positions; in addition, since the average La2–O distances are equal or larger than the La1–O ones (Tables 3 and 4 in the Supporting Information) there is no steric reason for the location of lithium close to La2 ions. As discussed above, Ti^{+4} and Al^{+3} are notably displaced towards La1 (Tables 1 and 2 in the Supporting Information) inducing a positive-charge deficiency in the vicinity of the La2 layers; this is compensated by their higher population and by the location of lithium in this region of the structure. Alternatively, since Ti^{+4} and Al^{+3} ions are displaced from the center of the BO_6 octahedra towards the La-poor layer, if the Li ions were located near these La-poor sheets they will experience a stronger repulsive interaction with tetravalent Ti ions and trivalent Al ions. Since electrostatic interactions are long-range, interactions other than first-neighbor interactions must be considered. In this context, we have calculated the electrostatic potentials at both the actual position of lithium in the La-rich layer (0.75, 0.3574, 0.2619) and at the equivalent one near the La-poor layer (0.75, 0.120, 0.2619). As a main result of this simple calculation (without local relaxations) the former is much more adequate (site potential 0.8 eV) to locate lithium ions, because the electrostatic field at the latter site is significantly positive (site potential 3.9 eV), mainly due to the effect of tetravalent Ti^{+4} ions.

Low-temperature structure: To determine whether the structure and/or the microstructure are also affected by the actual temperature of the sample, we recorded a PND at 2 K of sample 01HT. This was chosen because for this sample the effect of the temperature of annealing is clearly observed (see Tables 1 and 2 in the Supporting Information). The final structural model at 2 K derived for this sample is presented in Table 2, whereas Table 4 shows some selected structural information, both tables are to be found in the Supporting Information.

The material does not suffer any structural transition down to 2 K, the structure remaining essentially unchanged. In fact, the tilting system of the BO_6 octahedra is the same to that observed at room temperature, though the tilting angles increase slightly. On the other hand, the $(Ti/Al)O_6$ octahedra are less distorted at low temperature, mainly due to the location of Ti^{+4} and Al^{+3} closer to the ideal position; their displacement towards the La1 sites being only 0.03 Å at 2 K. Lowering the temperature has virtually no effect on the distribution of La^{3+}, Li^+, and the vacancies along the $2a_p$-axis in the structure (Table 2 in the Supporting Information). As the temperature is lowered ionic diffusion becomes more and more limited, as the ions have not enough thermal energy for motion. Thus, only minor rearrangements of the ions should be expected. The intensity of the superstructure peaks (i.e., the (hkl) with $k=2n+1$, the superstructure $2a_p$ axis being b) are directly related to the different occupation of the La1 and La2 sites; hence the intensity of peaks such as (010) would be a good indication of the evolution of site occupation in this series of compounds. Figure 6 shows the superstructure (010) peak of the PND patterns corresponding to samples 01 LT and 01 HT (the latter sample was measured at room temperature and 2 K). The integral breadths of the peaks are also indicated. It is evident from Figure 6 that the quenching temperature is the decisive factor for determining the intensity and width of the superstructure peaks and, consequently, the different composition of the La/vacancy–Li layers and the microstructural effects. The higher the temperature of quenching, the less intense and broader the superstructure peaks are. The intensity of the (010) peaks is mainly related to the different degree of occupation of the La sites, in such a way that the larger this difference, the more intense the peak is. As Tables 1 and 2 show (Supporting Information), in sample 01 LT the population of La1 and La2 differs by 37%, whereas for sample

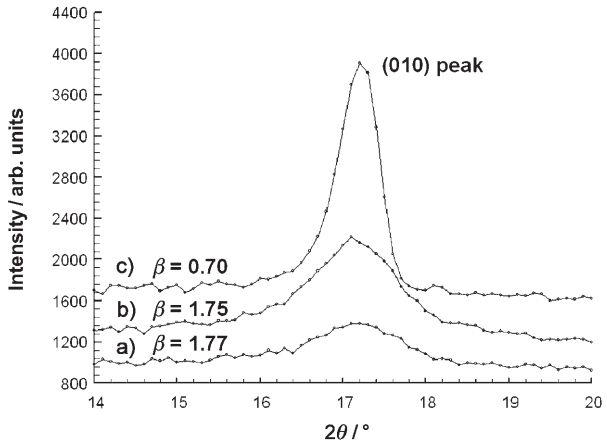

Figure 6. Superstructure (010) peak of the NPD patterns corresponding to sample 01 HT, measured at a) room temperature and b) 2 K; c) sample 01 LT measured at room temperature. The integral breadths ($\beta \times 10^3$ Å^{-1}) are also indicated.

01 HT this difference is 56 %. In contrast, the populations of both lanthanum sites in the sample quenched from 1573 K are the same, within the experimental error, at room temperature and at 2 K; as a result the intensity of the corresponding superstructure peaks are similar.

The peak width is related to microstructural effects, such as compositional or structural disorder, small-domain formation, stacking faults, and so forth (see next section). In contrast, if this structural disorder observed at room temperature were a thermally activated effect, that is, due to high ionic mobility, it should disappear as the temperature is lowered and ions are localized. As a result of this freezing of the ionic motion the material should be more ordered at low temperature and this should be reflected on the PND pattern, mainly in the superstructure peaks which should become sharper. However, this is certainly not the case, since the peaks breaths for sample 01 HT measured at room temperature and 2 K are almost the same. Thus, the dominant microstructural features in these oxides are not due to the motion of mobile ions (Li^+ in this case), but to "static" effects. As it will be shown in the next section, and previously reported[11] for other related compounds, the main microstructural effect in these oxides are the existence of microdomains and compositional fluctuations of the La/vacancy–Li layers, both being related to the distribution of the heavy and highly charged ions such as La^{+3} with a low mobility.

Still, some words must be devoted to comment the effect of lowering temperature on the position of lithium ions in the structure. As shown in Table 2 (in the Supporting Information), at low temperature lithium is located in positions similar to those occupied at room temperature, but slightly displaced towards the La2 sites. This is most likely due to the location of Ti^{+4} and Al^{+3} in the material: at 2 K they are closer to their ideal positions in the center of the BO_6 octahedra, (i.e., less displaced towards La1), than at room temperature, exerting an increased electrostatic repulsion over Li^+ ions, which then move in the opposite direction, towards La2.

Microstructure: Microstructure effects are numerous and usually appear superposed, thus the analysis of diffraction patterns to extract the real structure features is not simple; in fact it can be very complex. Parts (domains) of different size and shape and different orientations may be present; these domains may contain stacking faults and compositional fluctuations. Besides, inclusions and precipitates are just as frequent as stress and strain. Each of these real-structure features has its effect on the diffraction pattern. The limited size of the domains, and the presence of strain and stacking faults broaden the peaks; in addition, structural mistakes can also induce the displacement and asymmetry of some peaks.[27,28]

As previously reported,[11] $La_{2/3-x}Li_{3x}TiO_3$ materials have a complex microstructure that cannot be accounted for by the conventional models. To study the microstructure of these compounds we have used the two-step procedure proposed by Langford.[28,29] Each peak was fitted to a pseudo-Voigt function and the integral breadths ($\beta = A/I_0$, A = integrated intensity, I_0 = maximum of intensity) and the shape parameters (φ = FWHM/β; FWHM = full width at half maximum) were determined. The latter were checked to be within the theoretical limits for the Lorentzian ($\varphi = 0.6366$) and Gaussian ($\varphi = 0.9394$) functions, which the pseudo-Voigt function is built from; this ensures the method can be properly applied.

Figure 1 in the Supporting Information shows the Williamson–Hall plot[30] for sample 01 LT. The integral breadth of reflections with Miller indices $(0k0)$ (the b axis being the $2a_p$ one) are split into two groups. For those peaks with $k = 2n$, the breaths are dependent of the order, that is, they are d^*-dependent ($d^* = 1/d$, reciprocal spacing) indicating that, in this direction, there is some measurable contribution of microstrains or other kinds of "lattice distortions".[28] In contrast, those $(0k0)$ reflections with $k = 2n+1$ are much broader, their breadths being apparently independent of the order; in these cases the peak widths are dominated by domain size effects, the contribution of strains being masked. On the other hand, the $(h0h)$, $(h00)$ and $(00h)$ reflections show a clear dependence on d^*.

Thus, along the $\langle 101 \rangle$ directions the material would have microstrains. According to Langford[29] and Halder and Wagner[31] the contributions to the integral breadth of strains and domain size can be separated using Equation (1),[1] in which ε gives the mean apparent domain size and η is a measure of the strain related with the root mean square strain (e_{rms}) by $e_{rms} \sim \eta/5$).[32]

$$(\beta/d^*)^2 = \varepsilon^{-1}\beta/(d^*)^2 + (\eta/2)^2 \quad (1)$$

By using Equation (1) the domain size and shape can be obtained. Therefore, along the [100] and [001] directions the domains are about 20000(800) Å.

In addition, by using Equation (1) the domain size along the b axis can be estimated as $\langle D \rangle[010] = 4000(300)$ Å, and the domain size contribution to the breadth of the (010) peak was estimated to be $\beta_{(010)} = 1.3(8) \times 10^{-4}$ Å^{-1}. The extra breadth of $(0k0)$ reflections with $k = 2n+1$, such as (010) ($\beta_{(010)} = 9.5(8) \times 10^{-4}$ Å^{-1}), may be due to the presence of structural mistakes along the b axis. There are several different kinds of structure mistakes that contribute to peak breadth. Bearing in mind the structure of these materials (Figure 4), it is possible to propose a mechanism for these structure mistakes. They are most likely due to compositional fluctuations of the A-sites layers along the $2a_p$ axis. This kind of mistake broadens the $(0k0)$ PEAKS with $k = 2n+1$ and may produce shifts with respect to the positions determined from the unit cell, as observed in our patterns.[26,28] Small variations of the composition of the A-sites layers have neither effect in the intensities, nor in the integral breadths of the $(0k0)$, with $k = 2n$, peaks. In contrast, small variations in the occupancies of the A-sites have a significant relative effect in the intensities and breadths of the $(0k0)$, $k = 2n+1$, reflections.[11]

The total breadth of the $(0k0)$, $k = 2n+1$, reflections can be expressed as Equation (2),[11] in which $\beta^S_{(02n+10)}$ and

$\beta^{m}_{(02n+10)}$ are the contributions due to domain size effects and structural mistakes, respectively.

$$\beta_{(02n+10)}=\beta^{S}_{(02n+10)}+\beta^{m}_{(02n+10)} \quad (2)$$

Since $\beta^{S}_{(010)}$ can be estimated as $1.3(8)\times10^{-4}$ Å^{-1} and $\beta_{(010)}=9.5(8)\times10^{-4}$ Å^{-1}, then $\beta^{m}_{(010)}$ is $(9.5\text{–}1.3)\times10^{-4}$ Å^{-1} = $8.2(8)\times10^{-4}$ Å^{-1}. In a previous paper we derived the relationship between $\beta^{m}_{(02n+10)}$ and the probability (α) of compositional mistakes to occur along the $2a_p$ axis and the degree of local disorder between two neighboring layers (δ).[11] Remarkably, a combination of high probability ($\alpha\sim1$) and large compositional fluctuation ($\delta\sim0$) gives rise to very broad and weak ($02n+10$) reflections. The low value of $\beta^{m}_{(010)}$ ($8.2(8)\times10^{-4}$ Å^{-1}) and the relatively high intensity of the ($0k0$) reflections with $k=$ odd (including the (010), see Figures 3 and Figure 6), suggest that the composition of A-site layers are very close to the average values in Table 1 in the Supporting Information; fluctuations from those values are infrequent.

To summarize, the microstructure of sample 01 LT is composed of domains lamellar in shape with a basal plane of about (20000×20000) Å^2 on the {101} planes and a height around 4000 Å along the $2a_p$ axis (b axis). Also, subtle compositional fluctuations occur along the b axis in a few A-site layers within each domain. Finally, the misfit between the (101) spacing and the (010) spacing (they differ by 0.3%) induces some strain in the $\{h0h\}$ planes and also in the $\{02n+10\}$ ones, though in this case other microstructural effects (domain size and compositions fluctuations) are dominant.

For all the other samples studied, the resolution of the conventional X-ray diffractometers and a severe and generalized peak broadening (still more important for reflections with the k-Miller index odd) preclude the analysis of the microstructure in the way described above. We have not enough information to construct the corresponding Williamson–Hall plots; therefore, to study the microstructure of these compounds we have applied the procedure proposed by Langford,[28,32] which through using the graphic representation of Equation (1) (the so-called Langford plot of the sample) allows us to estimate the domain size and strains. As an example, Figure 2 in the Supporting Information shows this plot for sample 01 HT; assuming a spherical (isotropic) shape of the domains we obtained the values of the isotropic diameter, $\langle D_{iso}\rangle$, collected in Tables 3 and 4 in the Supporting Information.

The size effects seem to dominate the microstructure in all directions, though the low intensity of ($0k0$), $k=2n+1$, and a large value of the breadth of (010) peaks (the only of its class with measurable intensity in the PXRD patterns of all samples to be properly fitted) suggest that the compositional fluctuations of the A-site layers along the b axis may be very important ($\delta\sim0$) and the frequency of mistakes very high ($\alpha\sim1$) in all these samples.

The temperature of quenching seems to have an important influence on the domain size for samples with a high number of vacancies in the A-site layers. In this sense, for composition $La_{2/3}Li_{0.1}\square_{0.23}Ti_{0.9}Al_{0.1}O_3$, a reduction of the domain size is observed when compared samples 01 LT and 01 HT, (although both of them present relatively large domains, in agreement with the HRTEM results).

The effect of the composition is even more relevant. In the series of samples annealed at 1273 K, the domain size decreases as x increases (the number of vacancies decreases). The need to accommodate two ions of very different nature—size and charge—such as La^{+3} and Li^{+} together with vacancies within the A-sites of the structure might be related to this fact: as x increases, the A-site layers are more populated and the ability of the structure to accommodate lanthanum and lithium ions in the same layer is reduced; therefore, the formation of small domains, or microdomains, might allow the ions and vacancies to accommodate in the domains boundaries which may present a local structure significantly different of that of the average one.

Thus, if the number of vacancies is low, the samples will present small domains even for low annealing temperatures and increasing the quenching temperature will have slight or no effect on the microstructure, because the driving force for the formation of small or micro domains is not the temperature but the sample composition. These results are in agreement with the variation of domain sizes with the composition and annealing temperature of the samples observed by HRTEM for these oxides.

Electrical properties: Figure 7 shows the variation of the bulk Li^{+} conductivity at 295 K for both series of $La_{2/3}Li_x$-$Ti_{1-x}Al_xO_3$ samples, (quenched from 1273 and 1573 K), depending on x. The conductivity increases with increasing lithium content up to a value corresponding to $x=0.25$ for both curves. However, it seems that the ionic conductivity depends on the thermal treatment when the annealing and quenching temperature influences on the microstructure of the sample: the ionic conductivity depends on the thermal treatment for the oxides with $0.15<x<0.3$ but it does not for the compounds with $x\leq0.15$ and $x=0.3$. The crystal

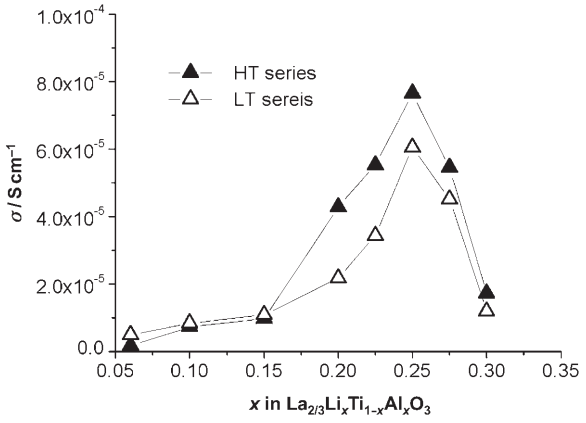

Figure 7. Variation of the bulk Li^{+} conductivity with x at 295 K for $La_{2/3}Li_xTi_{1-x}Al_xO_3$ samples annealed and quenched from 1273 K.

structure of the oxides with $0.15 < x < 0.3$ is not modified by the thermal treatment (Tables 1 and 2 in the Supporting Information), but the sample microstructure is.

Therefore, the variation of the ionic conductivity with the thermal treatment of the samples is due to modifications of their crystal microstructure in such a way that the ionic conductivity is higher for the oxides with microdomain formation than for the oxides formed by relatively large domains. In this sense, sample 02HT (microdomains) has higher ionic conductivity than 02LT (large domains), both with $x = 0.2$; however, the crystal structure is similar for both quenching temperatures.

It is worth mentioning that a number of authors have reported the dependence of the bulk lithium conductivity on the thermal treatment of samples of $La_{2/3-x}Li_{3x}TiO_3$ titanates, but they did not relate this fact with the microstructure of the materials,[33–35] as clearly shown in here.

Conclusion

The study of the crystal structure of some $La_{2/3}Li_xTi_{1-x}Al_xO_3$ oxides ($x = 0.1$, 0.2, and 0.3) annealed and quenched from two different temperatures (1273 K and 1573 K) has been carried out by means of the combination of averaging (PND and PXRD) and local (SAED and HRTEM) techniques.

SAED and HRTEM indicate that all the oxides have perovskite-related unit cell of dimensions $\sim\sqrt{2}a_p \times \sim 2a_p \times \sim\sqrt{2}a_p$ and a complex microstructure consisting of domains of ordering with three different perpendicular orientations of the $2a_p$ axis. However, the size of the domains depends on the composition and the annealing temperature of the sample: in general, the oxides with high concentration of vacancies present large domains and those with low concentration of vacancies have a microdomain microstructure; in addition, high annealing temperatures also tend to lead to the formation of microdomain microstructures.

The crystal microstructure of the materials has been taken into account to refine their crystal structure. The results of these refinements reveal that the formation of the perovskite-type superstructure is due to tilting of the $(Ti/Al)O_6$ octahedra and ordering of the La/vacancy–Li layers along the [0 1 0] direction.

All the oxides have the same octahedra tilting system ($a^-b^0a^-$), but the value of the tilting angles depends on the composition, in such a way that the higher the occupation of the A-sites, the larger the octahedra tilting. However, the annealing temperature does not affect the tilting angles. The $(Ti/Al)O_6$ octahedra are also distorted.

The lithium ions are not located at the same position as the La^{3+} ions (i.e., the A positions of the perovskite structure) but at interstitial positions, in such a way that their coordination polyhedra is a square pyramid with lithium ion at the apex. Therefore, there is a large amount of non-occupied interstitial positions of this kind for the lithium ions to move to, and this is likely to be the reason for the very high ionic conductivity of these kinds of materials ($\sim 8\times10^{-5}\ \Omega^{-1}\,cm^{-1}$ for the oxide with $x = 0.25$ (or even higher for other similar systems[36] for which a similar situation should operate).

The ordering of the La^{3+} ions and vacancies (situated at the A-positions) along the $2a_p$ axis depends mainly on the composition. In the oxide with $x = 0.1$ (the one with the highest amount of vacancies), there are lanthanum-rich (La2) (or vacancy-poor) layers alternated with lanthanum-poor (La1) (or vacancy-rich) layers. However, in the oxide with $x = 0.3$, the composition of the two layers is similar. The Ti^{4+} and Al^{3+} ions are displaced from the ideal B perovskite positions towards the La1 layers.

The thermal treatment of the samples mainly affects to their microstructure, in particular to the ordering domains size. Apart from the ordering domain formation, other microstructural "mistakes", such as compositional fluctuations along the $2a_p$ axis and strains, are deduced by analysis of the PXRD data.

The lithium ion conductivity of the $La_{2/3}Li_xTi_{1-x}Al_xO_3$ materials depends on their composition and microstructure. The conductivity increases with lithium content up to a value corresponding to $x = 0.25$ and it is higher for those oxides with a microdomain microstructure. This is indeed an interesting result that goes far beyond the classical structure–property relationship paradigm.

Experimental Section

Three oxides of the $La_{2/3}Li_xTi_{1-x}Al_xO_3$ system with different compositions (corresponding to $x = 0.1$, 0.2, and 0.3), enriched with ^6Li, were prepared from stoichiometric amounts of $^6Li_2CO_3$ (Aldrich), La_2O_3 (Aldrich 99.999%), TiO_2 (Aldrich 99.99%) and Al_2O_3 (Aldrich 99.99%). La_2O_3 was heated overnight at 1273 K and TiO_2 and Al_2O_3 at 973 K prior to weighing. The mixtures were ground and then heated in Pt boats for 6 h at 1173 K for decarbonation. Afterwards, the samples were reground, pelleted, covered with powder of the sample of the same composition to prevent lithia loss, and fired at 1373 K for 12 h followed by further grinding, repelleting, and refiring at 1573 K for another 12 h. After preparation, two different thermal treatments were carried out for each oxide: annealing of the samples at 1273 K for 12 h and quenching from this temperature (LT series) and annealing at 1573 K for 12 h, (HT series), and afterwards quenching in both cases on a brass plate to ensure a high cooling rate. All thermal treatments were performed in air.

Crystalline phase identification was done by powder X-ray diffraction by using a Philips X'PERT diffractometer with $Cu_{K\alpha1}$ radiation ($\lambda = 1.5406$ Å) and with a curved Cu monochromator.

Chemical analysis of the compounds was performed by inductively coupled plasma (ICP) spectroscopy by using a JY-70 plus instrument. The samples were dissolved with a mixture of nitric, hydrochloric, and hydrofluoric acids in a 3:2:1 molar ratio at 150 °C in a high-pressure Teflon reactor fitted with a temperature sensor and placed inside of a MILESTONE microwave digestion furnace (ASM-1200 model). The results of the analysis indicated good agreement between analytical and nominal values.[8]

For transmission electron microscopy, the samples were ground in *n*-butyl alcohol and ultrasonically dispersed. A few drops of the resulting suspension were deposited on a carbon-coated grid. SAED studies were performed with an electron microscope JEOL 2000FX (double tilt ±45°) working at 200 kV and HRTEM studies with an electron microscope JEOL 400EX (double tilt ±25°) working at 400 kV. The chemical composition of the crystals (atomic ratio of La, Ti and Al) was analyzed by

EDS with the JEOL 2000FX microscope, in good agreement with the nominal composition.

The samples of both LT and HT series were studied by powder neutron diffraction (PND) at room temperature on the diffractometer G4.2 of the Orphée Reactor at Laboratoire Léon Brillouin. A monochromatic beam of wavelength 2.3251 Å was selected with a Ge (004) monochromator; for this radiation the instrumental resolution is within the range $2.7\times10^{-3}\leq(\Delta Q/Q)\leq0.022$. In addition, sample 01HT was also measured at 2 K to determine the static or dynamic origin of the structural disorder present in these materials. The structural refinements were carried out by the Rietveld method using the FullProf program.[37] In some cases, a severe microstructural contribution to the profile had to be considered and we undertook the refinement of the structures of our materials taking into account the effects of their microstructure on the diffraction patterns. We applied a phenomenological approach using a new capability of the FullProf[37] program, which allows some of the peaks to be described by their own breadths and shapes, as well as small displacements from their positions calculated from the average unit cell. Prior to the structure refinements, a pattern matching without a structural model was performed. This allowed us to obtain suitable profile parameters, including the breadths, shapes, and displacements of those reflections with relevant microstructural contributions. Then, the structural model was refined keeping the profile parameters constant. If needed during refinement, some of these profile parameters were allowed to vary; however, at the final steps of the refinements they were kept constant. The refinements were stable provided the number of refined parameters describing the structural model was low enough to obtain an adequate peak-to-parameter ratio. To ensure this, isotropic thermal factors (ITF) were used for all the atoms in the structure and some constrains were used. The fitting process was finished when convergence was reached.

Some microstructural features of the materials were obtained from precise diffraction data obtained on a Bruker D8 high-resolution X-ray powder diffractometer, by using monochromatic $Cu_{K\alpha1}$ ($\lambda=1.5406$ Å) radiation obtained with a germanium primary monochromator, and equipped with a position sensitive detector (PSD) MBraun PSD-50M. The measured angular range, the step size, and counting times were selected to ensure enough resolution (the step size should be at least, 1/10 of the FWHMs) and statistics. The instrumental contribution to line broadening was evaluated by using an NIST LaB_6 standard reference material (SRM 660a; $\mu=1138\,cm^{-1}$, linear absorption coefficient for $Cu_{K\alpha1}$ radiation). The study of the microstructure of the samples was performed by the two-step procedure proposed by Langford and Louër.[28,29,32]

Impedance measurements were performed in an impedance/gain phase analyzer Solartron 1255 A with dielectric interface 1296. Pellets of about 13 mm diameter and 2 mm thickness were prepared by pressing the powder samples and sintering at 1573 K. After sintering, the pellets were annealed at 1573 or 1273 K over a period of 12 h and were rapidly cooled by removing from the furnace. Electrodes were made by coating opposite faces with platinum paste and heating to 1123 K over 2 h. Measurements were carried out in air at 298 K in a frequency range from 1×10^{-3} to 6×10^{6} Hz.

Acknowledgements

We thank Ministerio de Educación y Ciencia for funding the projects MAT2004-03070-C05-01 and MAT2004-03070-C05-05 and CAM for the project MATERYENER S-505/PPQ/0358. The access to the neutron facilities at the Laboratoire Léon Brillouin was supported by the ARI action of the HPRI Program of the European Community. We also thank the Microscopy Centre "Luis Bru" from U.C.M. for technical assistance.

[1] R. Newnham, *Structure Property Relations*, Springer, Berlin, **1974**.
[2] A. G. Belous, G. N. Novitkaya, S. V. Polyanetskaya, Y. I. Gornikov, *Izv. Akad. Nauk. SSSR, Neorg. Mater.* **1987**, *23*, 470.
[3] Y. Inaguma, C. Liquan, M. Itoh, T. Nakamura, *Solid State Commun.* **1993**, *86*, 689.
[4] H. Kawai, J. Kuwano, *J. Electrochem. Soc.* **1994**, *141*, L78.
[5] Y. Inaguma, C. Liquan, M. Itoh, T. Nakamura, *Solid State Ionics* **1994**, *70–71*, 196.
[6] Y. Inaguma, M. Itoh, *Solid State Ionics* **1996**, *86–88*, 257.
[7] S. Stramare, V. Thangadurai, W. Weppner, *Chem. Mater.* **2003**, *15*, 3974.
[8] A. Morata-Orrantia, S. García-Martín, E. Morán, M. A. Alario-Franco, *Chem. Mater.* **2002**, *14*, 2871.
[9] A. Morata-Orrantia, S. García-Martín, M. A. Alario-Franco, *Chem. Mater.* **2003**, *15*, 3991.
[10] S. García-Martín, A. Morata-Orrantia, M. H. Aguirre, M. A. Alario-Franco, *Appl. Phys. Lett.* **2005**, *86*, 043110.
[11] S. García-Martín, M. A. Alario-Franco, H. Ehrenberg, J. Rodríguez-Carvajal, U. Amador, *J. Am. Chem. Soc.* **2004**, *126*, 3587.
[12] A. Várez, Y. Inaguma, M. T. Fernández-Díaz, J. A. Alonso, J. Sanz, *Chem. Mater.* **2003**, *15*, 4637.
[13] A. Várez, M. T. Fernández-Díaz, J. A. Alonso, J. Sanz, *Chem. Mater.* **2005**, *17*, 2404.
[14] M. Yashima, M. Itoh, Y. Inaguma, Y. Morii, *J. Am. Chem. Soc.* **2005**, *127*, 3491.
[15] J. L. Fourquet, H. Duroy, M. P. Crosnier-López, *J. Solid State Chem.* **1996**, *127*, 283.
[16] A. Várez, F. García-Alvarado, E. Morán, M. A. Alario-Franco, *J. Solid State Chem.* **1998**, *118*, 78.
[17] A. M. Glazer, *Acta Crystallogr. Sect. B* **1972**, *28*, 3384.
[18] A. M. Glazer, *Acta Crystallogr. Sect. A* **1975**, *31*, 756.
[19] P. M. Woodward, *Acta Crystallogr. Sect. B* **1997**, *53*, 32.
[20] M. Sommariva, M. Catti, *Chem. Mater.* **2006**, *18* , 2411.
[21] C. J. Howard, H. J. Stokes, *Acta Crystallogr. Sect. B* **1998**, *54*, 782.
[22] R. D. Shannon, *Acta Crystallogr. Sect. A* **1976**, *32*, 751.
[23] J. A. Alonso, J. Sanz, J. Santamaría, C. León, A. Várez, M. T. Fernández-Díaz, *Angew. Chem.* **2000**, *112*, 633; *Angew. Chem. Int. Ed.* **2000**, *39*, 619.
[24] Y. Inaguma, T. Katsumata, M. Itoh, Y. Morii, *J. Solid State Chem.* **2002**, *166*, 67.
[25] J. Sanz, J. A. Alonso, A. Várez, M. T. Fernández-Díaz, *J. Chem. Soc. Dalton Trans.* **2002**, *7*, 1406.
[26] R. L. McGreevy, *J. Phys. Condens. Matter* **2001**, *13*, R877.
[27] B. E. Warren, *X-Ray Diffraction*, Dover Publications, New York, **1990**.
[28] J. I. Langford in *Defect and Microstructure Analysis by Diffraction, IUCR Monographs on Crystallography 10* (Eds.: P. Snyder, F. Fiala, H. Bunge), Oxford University Press: Oxford, **1999**, pp. 59–81.
[29] J. I. Langford, *NIST Special Publication 846*; *Proceedings of the International Conference "Accuracy in Powder Diffraction II"*, Gaithersburg, MD, **1992**.
[30] G. K. Williamson, W. H. Hall, *Acta Med. Biol.* **1953**, *1*, 22.
[31] N. C. Halder, C. N. Wagner, *Adv. X-Ray Anal.* **1966**, *9*, 91.
[32] D. Louër, in *Defect and Microstructure Analysis by Diffraction, IUCR Monographs on Crystallography 10* (Eds.: P. Snyder, F. Fiala, H. Bunge), Oxford University Press, Oxford, **1999**, p. 671.
[33] Y. Harada, T. Ishigaki, H. Kawai, J. Kuwano, *Solid State Ionics* **1998**, *108*, 407.
[34] C. W. Ban, G. M. Choi, *Solid State Ionics* **2001**, *140*, 285.
[35] A. Várez, J. Ibarra, A. Rivera, C. León, J. Santamaría, M. A. Laguna, M. L. Sanjuán, J. Sanz, *Chem. Mater.* **2003**, *15*, 225.
[36] A. Morata-Orrantia S. García-Martín, M. A. Alario-Franco, *Chem. Mater.* **2003**, *15* , 3991.
[37] J. Rodríguez-Carvajal, *Physica B* **1993**, *19*, 55; the program and manual can be found at http://www-llb.cea.fr/fullweb/powder.htm.

Received: February 9, 2007
Published online: April 5, 2007

